Journal of
Materials Chemistry A

Accepted Manuscript

This is an *Accepted Manuscript*, which has been through the RSC Publishing peer review process and has been accepted for publication.

Accepted Manuscripts are published online shortly after acceptance, which is prior to technical editing, formatting and proof reading. This free service from RSC Publishing allows authors to make their results available to the community, in citable form, before publication of the edited article. This *Accepted Manuscript* will be replaced by the edited and formatted *Advance Article* as soon as this is available.

To cite this manuscript please use its permanent Digital Object Identifier (DOI®), which is identical for all formats of publication.

More information about *Accepted Manuscripts* can be found in the **Information for Authors**.

Please note that technical editing may introduce minor changes to the text and/or graphics contained in the manuscript submitted by the author(s) which may alter content, and that the standard **Terms & Conditions** and the **ethical guidelines** that apply to the journal are still applicable. In no event shall the RSC be held responsible for any errors or omissions in these *Accepted Manuscript* manuscripts or any consequences arising from the use of any information contained in them.

Modulating the atomic and electronic structure through alloying and heterostructure of single-layer MoS_2

Xiao-Lin Wei[a,b], *Hui Zhang*[b,c], *Gen-Cai Guo*[a], *Xi-Bo Li*[b], *Woon-Ming Lau*[b,c], *Li-Min Liu*[b*]

[a] *Laboratory for Quantum Engineering and Micro-Nano Energy Technology, Department of Physics, Xiangtan University, Xiangtan, Hunan 411105, China*
[b] *Beijing Computational Science Research Center, Beijing 100084, China.*
[c] *Normal college, Shenyang University, Shenyang 110044, China*
[d] *Chengdu Green Energy and Green Manufacturing Technology R&D Center, Chengdu, Sichuan, 610207, China*

* Email: limin.liu@csrc.ac.cn

Abstract

Among dozens of transition metal dichalcogenides (TMDs), single-layer MoS_2 with a direct band gap has attracted great attention because of their potential applications. In this work, the atomic structures and electronics properties of mixed alloys or heterostructures of TMDs with single-layer MoS_2 are explored based on the density functional theory (DFT). The calculated quasi-binary phase diagrams reveal that different alloyed TMDs have great distinct stability and band structures, and the band gap of single-layer MoS_2 can be tuned from 0.89~1.87 eV by either alloys or heterostructures with other TMDs. Heterostructures between TMDs not only can tune the band gap, but also modulate band edge position to enhance the photocatalytic activity. More fascinatingly, the MoS_2-WS_2 heterostructure exhibits the unique electronic properties of spontaneous electron-hole separation. Such result not only reveals that both alloyed or heterostructures can effectively tune the electronics of TMDs, but also it will stimulate the further work to design the new type of photocatalysts.

1. Introduction

In the past few years, the discovery of graphene[1] has intrigued tremendous studies on novel low-dimensional materials[2-5]. The research on single-layer transition metal dichalcogenides (TMDs) is extremely active due to its unique properties. For example, bulk MoS_2 is semiconducting with an indirect band gap, while single-layer MoS_2 becomes a semiconductor with a direct gap due to quantum confinement [6,7], which induces many novel properties, such as strong photoluminescence and absorption[8-10]. The TMDs have a formula of TX_2 and could occur in more than 40 different types depending on the combination of transition metal (T=Mo, W, Cr, V, etc.) and chalcogen (X=S, Se, Te, etc.). The electronic structures of TMDs vary from metallic (e.g. NbS_2 and VS_2) to semiconducting (e.g. MoS_2 and WS_2).[11-14] The versatility of electronic structure in TMDs offers opportunities for fundamental and technological research in a variety of fields.

MoS_2 have many potential applications in a variety of fields including hydrogen production from water[15], rechargeable batteries[16], and electronic devices such as field-effect transistors[17]. The prosperous research on MoS_2 also focus on exploring the fabrication[18], band gap engineering[19-21], nanoribbons[22-25], defects[26-28] and grain boundaries[29,30]. The 2D composites could exhibit unexpected properties，which are absent in the constituents. Recently, a nonvolatile memory cell based on MoS_2/graphene heterostructures has been fabricated.[31] Synergetic effect of MoS_2 with other materials, such as graphene, TiO_2, and CdS, leads to enhanced photocatalytic H_2 production activity of cocatalysts.[32-34] Owing to the structure similarity of TMDs, MoS_2 may be easily alloyed with other TMDs. In addition, the versatility of TMDs provides a new route to obtain rich electronic structures by fabricating TMD complexes. Condensing the dozens of TMD types, it is natural to think whether is possible to tune the electronic properties by alloying MoS_2 with other TMDs, which has the great potential to modulate the electronic structures and enhance efficiency of actual applications.

Although TMDs alloys[35-37] and heterostructures[38-40] have been recently investigated, the phase stability of mixed TMDs has been seldom explored. The composites might have distinct atomic structures from their corresponding bulks. If the two constituents of the two phases have good structure similarity, they may prefer to form homogenous alloys (solid solutions), and the two types of metal atoms will randomly occupy the corresponding sites in this kind of system, otherwise if the solid solutions is thermodynamically unstable, they prefer to form heterostructures [41-43]. In addition, the atomic structures significantly affect electronic structure of alloyed TMDs. The detailed phase stability and their corresponding electronic properties of alloyed TMDs are crucial for designing TMDs composites.

In this paper, the atomic configurations of single-layer alloyed TMDs ($Mo_{1-x}W_xS_2$, $Mo_{1-x}Cr_xS_2$, and $Mo_{1-x}V_xS_2$) and heterostructures are carefully studied by first-principle calculations. The results clearly demonstrate that $Mo_{1-x}W_xS_2$ alloys prefer to form hetero-atom (Mo-W) bonds, whereas $Mo_{1-x}Cr_xS_2$ and $Mo_{1-x}V_xS_2$ alloys tend to form homo-atom (Mo-Mo, Cr-Cr, and V-V) bonds. The calculated quasi-binary phase diagrams further predict that $Mo_{1-x}W_xS_2$ alloys have high stability,

but $Mo_{1-x}Cr_xS_2$ and $Mo_{1-x}V_xS_2$ exhibit severe phase segregations. Besides the atomic configurations, band gaps of TMD alloys and heterostructures can be tuned with a wide range of 0.89~1.87 eV. The MoS_2-WS_2 heterostructures has the decent band gap and the suitable band edge positions, and especially the MoS_2-WS_2 heterostructures exhibit the extraordinary electronic properties of spontaneous electron-hole separation. Such result not only provides a novel way to tune the band structure of TMDs, but also it will help to design the high efficient photocatalysts.

2. Methods

The first-principles calculations were performed with the Vienna Ab Initio Simulation Package (VASP)[44,45]. Projector-augmented-wave (PAW) potentials[46] were used to account electron-ion interactions. The generalized gradient approximation (GGA) with the PBE functional[47] was used to treat the electron exchange correlation interactions. To remove spurious interactions between neighboring structures due to periodic calculations, a vacuum layer of no less than 12 Å was taken in the perpendicular direction when necessary. The energy cutoff was set to 400 eV and Monkhorst-Pack scheme was used to sample Brillouin zone (BZ)[48]. The 18×18, 4×4, 8×1, and 16×1 K-meshes were employed for pure TMDs, alloys and heterostructures, respectively. The equilibrium geometries were fully optimized with both the lattice vectors and atom coordinates relaxed with the tolerance of less than 0.01eV/angstrom on each atom.

For ordinary binary in $A_{1-x}B_x$ alloys, atoms A and B randomly occupy the lattice sites. For these present quasi-binary $Mo_{1-x}T_xS_2$, A and B represent Mo and other alloying transition metals T (W, Cr, and V), respectively. The sulphur atoms locate at the original trigon lattice, whereas the Mo and T atoms randomly share the metal sites. Simulation of the substitutional alloys is complicated due to the random distribution of atoms. It conventionally needs very large supercells to represent substitutional alloys. For the simplest case of a binary system with total N sites, there are 2^N possible atomic configurations whose total energy needs to be structurally relaxed, and then averaged. In this paper, we use the special quasi-random structures (SQSs) method proposed by Zunger et al[49] as a computationally efficient way to describe this random distribution. The random alloys can be directed modeled by the specially designed small periodic structures with selective occupation of the N lattice sites by A and B atoms which mimic, for finite N, the correlation functions of an infinite substitutional random alloy fairy closely. For a binary substitution alloy $A_{1-x}B_x$, if the site is occupied by A or B atom, the value is i=+1 or -1. The correlation functions are described as $\overline{\Pi}_{k,m}$, where k=2, 3…, represent the pair, triple correlation functions, etc., and m=1, 2, 3 …, represent the first, second and third-nearest distance, etc. The correlation functions of ideal $A_{1-x}B_x$ alloys are $\overline{\Pi}_{k,m} = (2x-1)^k$.

In the present calculations, a (4×4) supercell is used, which contains 16 basic units of TS_2 or a total of 48 atoms. The initial configurations of $Mo_{1-x}T_xS_2$ at x=0.5 and 0.25 were generated using SQSs technique. It should be noted that the structure of $Mo_{0.25}T_{0.75}S_2$ is the same as that of $Mo_{0.75}T_{0.25}S_2$ with the exchange of atom types

between Mo and T. Thus from this, five structural data can be collected: x=0, 0.25, 0.5, 0.75 and 1. The correlation function $\overline{\Pi}_{2,1}$ can be redefined as $\overline{\Pi}_{2,1} = \frac{1}{N_{\text{bond}}} \sum_{j,k=1,N}^{j>k} i_j i_k$, where N_{bond} represents the number of possible neighboring bonds between metals. For a supercell of $Mo_{1-x}T_xS_2$, the total number of neighboring bonds of A-A, A-B and B-B, N_{AA}, N_{AB} and N_{BB}, have the following formulas:

$$(N_{AB} + 2N_{AA}) / Z = N_A = N(1-x) \quad (1)$$

$$(N_{AB} + 2N_{BB}) / Z = N_B = Nx \quad (2)$$

where N and Z are the total number and the coordination number of metal atoms and equal to 16 and 6 here. As a result, the correlation function can be calculated by

$$\overline{\Pi}_{2,1} = \frac{N_{AA} + N_{BB} - N_{AB}}{N_{AA} + N_{BB} + N_{AB}} = 1 - 4x + \frac{8N_{BB}}{NZ} = 1 - 4x + \frac{N_{BB}}{12} \quad (3)$$

The correlation function can be completely defined by N_{BB}. In the ideal solutions of $Mo_{1-x}T_xS_2$, the correlation functions are $\overline{\Pi}_{2,1}(\text{Ideal}) = (2x-1)^k$, and the ideal neighboring bond number is $N_{BB} = \frac{1}{2}x^2 NZ = 48x^2$. The SQSs which were finally chosen to model the random alloys have the correlations functions identical with the ideal solutions up to the nearest neighboring pairs $\overline{\Pi}_{2,1}(\text{SQS}) = \overline{\Pi}_{2,1}(\text{Ideal})$ and N_{BB} equals to 3, 12, and 27 for x=0.25, 0.5, and 0.75. We refer these SQSs as SQS-16 in the following.

3. Results and discussion

3.1 Atomic structure of pure TMDs

As shown in Fig. 1(a), the single-layer pure TS_2 (here, T=Mo, Cr, and V) has graphene-like 2D hexagonal lattice, referred as H-TS_2. The single-layer H-TS_2 exhibits a trigonal prismatic structure with a T atom layer sandwiched by two S atom layers with the sequence of S-T-S. The single-layer H-TS_2 belongs to P-6M2(D_{3h}) point group symmetry. The primitive cell contains three atoms, and T atom in Wyckoff site *1(a)* at (0, 0, 0) and S atoms in *2(h)* at (1/3, 2/3, ±Z). The calculated lattice constants are 3.18 Å, 3.18 Å, 3.06 Å, and 3.17 Å for MoS_2, WS_2, CrS_2, and VS_2, respectively. As shown in Fig. 1(b), MoS_2, WS_2, and CrS_2 are nonmagnetic-direct-band-gap semiconductors at Γ-Γ in BZ with gap of 1.68eV, 1.81eV, and 0.89 eV, respectively. We have checked Cr-Containing system with nonzero spin, and the results show no spin polarization for the Cr-Containing system. VS_2 is metallic and ferromagnetic due to the bands crossing the Fermi surface and spin-polarization, which agrees with the previous studies[13,50]. The calculated band gaps compare well with the available experimental values (1.9 eV of MoS_2[8] and 2.1 eV of WS_2[14]). It should be noted that pure DFT calculations usually underestimate the

band gap of semiconductor because of the self-interaction errors, and DFT+U approach or of hybrid functionals may give more accurate band gaps.[51] As for the single-layer MoS_2, the hybrid HSE06 functional gives the values of 2.05 eV, which is more close to the experimental value of 1.90 eV than that of 1.68 eV given by PBE functional. [52]

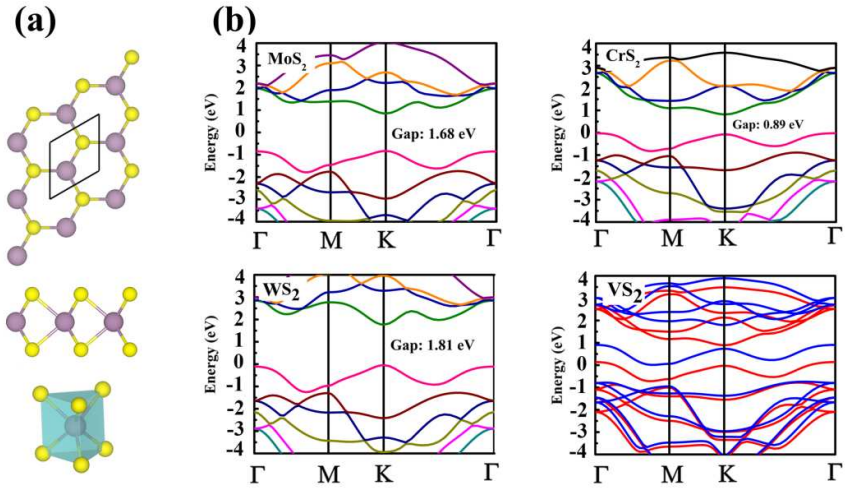

Fig. 1 *(a) Top, side and polyhedral views of atomic structure of monolayer TMD are shown from upper to lower panels. The purple and yellow balls represent T and S atoms, respectively. The unit cells are depicted by the black lines. (b) Band structures for the different TMDs: MoS_2, WS_2, CrS_2, and VS_2. The spin-up and –down bands of VS_2 are shown in red and blue due color, respectively. Band dispersions of other TMDs (MoS_2, WS_2, and CrS_2) are depicted with various colors.*

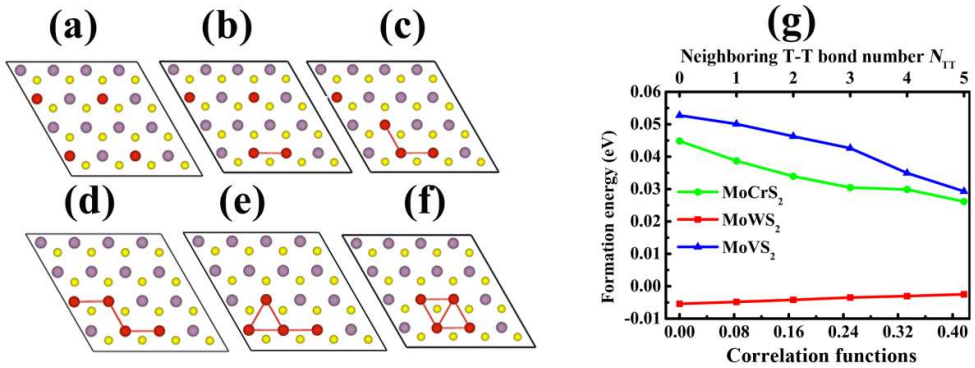

Fig. 2 *(a)-(f): Various possible configurations for $Mo_{0.75}T_{0.25}S_2$, and the corresponding neighboring T-T bonds are from 0 to 5. Here, the neighboring metal atom bonds are depicted by red lines in the right. (g) The formation energies as the functions of both correlation functions, $\overline{\Pi}_{2,1}$, and neighboring T-T bonds number, N_{TT}, are shown in. The intrinsic relationship between these two functions are: $\overline{\Pi}_{2,1} = \frac{N_{TT}}{12}$.*

3.2 Atomic configurations of the alloyed TMDs

The alloyed TMDs may exhibit many possible atomic configurations. A basic question of atomic arrangement is still rather complex. They can either form the homo or hetero phases. To solve this problem, the formation energies are calculated in order to compare the stability of the different atomic configurations. Alloys $Mo_{0.75}T_{0.25}S_2$ were chosen for this purpose because they have equal and less possible configurations compared with $Mo_{0.25}T_{0.75}S_2$ and $Mo_{0.5}T_{0.5}S_2$, respectively. In $Mo_{0.75}T_{0.25}S_2$ with total 4 T atoms, minimum 0 and maximum 5 neighboring T-T bonds can be formed. The atomic configurations are shown in Fig. 2(a)-(f). The formation energies of $Mo_{0.75}T_{0.25}S_2$ with various atomic configurations, calculated by $\Delta E = E(\mathrm{Mo_{0.75}T_{0.25}S_2})\text{-}0.75*E(\mathrm{MoS_2}) - 0.25*E(\mathrm{TS_2})$, are shown in Fig. 2(g). Considering the huge computational requirement of calculating all the configurations, only the typical configurations are considered. And the reliability of such way is further checked. For examples, two more configurations of $Mo_{0.75}Cr_{0.25}S_2$ are considered: One has three T atoms connected in a straight line (Fig. S1(a)), and the other has two separated pairs of neighboring T atoms(Fig. S1(b)). The total energies of them line between those of configuration in Fig. 2(b) and (d). In addition, the energy difference between the two configurations in Fig. S1 and that in Fig. 2(c) is equally small and less than 2 meV. Such result indicates that the choice of the configurations is reliable.

$Mo_{1-x}T_xS_2$ alloys have excess hetero-atom (Mo-T) bonds and correspondingly reduced homo-atom (Mo-Mo and T-T) bonds than pure TS_2. Besides, the more T-T bonds formed in alloys imply both more homo-atom bonds (Mo-Mo and T-T) and less hetero-atom bonds (Mo-T). The formation energy will be negative if the bond energy of hetero-atom bonds is higher than that of homo-atom bonds, otherwise will be positive. Thus the atomic arrangement tendency can be easily reflected by only whether the formation energy is positive or negative. As shown in Fig. 2(g), $Mo_{0.75}W_{0.25}S_2$ alloys possess negative formation energies, which indicate that the bond energy of hetero-atom bonds is higher than that of homo-atom bonds. That is to say, $\Delta E_{\mathrm{MoT}} > \frac{1}{2}(\Delta E_{\mathrm{MoMo}} + \Delta E_{\mathrm{TT}})$. For such kind of alloys, the hetero atoms take priority of bonding together (Mo-W bonds) than homo atoms (Mo-Mo and W-W bonds). Different from that of $Mo_{0.75}W_{0.25}S_2$, the formation energies become positive for both $Mo_{0.75}Cr_{0.25}S_2$ and $Mo_{0.75}V_{0.25}S_2$ alloys. The positive formation energies indicate that the bond energy of hetero-atom is lower than that of homo-atom, meaning $\Delta E_{\mathrm{MoT}} < \frac{1}{2}(\Delta E_{\mathrm{MoMo}} + \Delta E_{\mathrm{TT}})$. In such alloys, the homo-atoms prefer to bonding together ((Mo-Mo, Cr-Cr and V-V bonds) than homo-atoms (Mo-Cr, Mo-V bonds).

Fig. 2(g) also explore that the formation energies change monotonously along with the bond T-T number $N_{\mathrm{T\text{-}T}}$. This feature clearly shows that the total energy of alloys can be simply determined by the number of neighboring metal-atom bonds. As $N_{\mathrm{T\text{-}T}}$ increases from 0 to 5, the formation energy increases from –0.005 eV to –0.002 eV for $Mo_{0.75}W_{0.25}S_2$, but decreases from 0.045 eV to 0.026 eV for $Mo_{0.75}Cr_{0.25}S_2$, and

from 0.053 eV to 0.029 eV for $Mo_{0.75}V_{0.25}S_2$. Such results clearly suggest clearly suggest a hetero-atom bonding preference of $Mo_{1-x}W_xS_2$ alloys, and homo-atoms segregation priority of $Mo_{1-x}Cr_xS_2$ and $Mo_{1-x}V_xS_2$ alloys.

3.3 Phase stability of TMD alloys

As mentioned in the method section, many possible configurations can be formed in TMD alloys, but the alloys with atoms randomly distributing become more stable at high temperatures due to higher entropy. The SQSs technique was used along with DFT calculations to model these alloys as described in the method section. The SQS-16 configurations are shown in Fig. 3(a), and the corresponding correlation functions are shown in the Table S1. These structures generated by SQSs have correlations functions identical with the random alloy up to the nearest neighboring pairs ($\bar{\Pi}_{2,1}(\mathrm{SQS}) = \bar{\Pi}_{2,1}(\mathrm{Ideal})$).

First, the interactions between long-distant neighbors generally contribute less to the total energy than that between nearest neighbors. Second, as the feature of formation energies changing monotonously with the number of neighboring homo-atom bonds has been demonstrated in the last part, the difference of total energies among various configurations are mainly dependent on neighboring nearest atoms. As a result, these SQSs we obtained are sufficient to model TMDs alloys.

In order to determine the phase stability of alloys $Mo_{1-x}T_xS_2$ with different compositions, the mixing enthalpy of $Mo_{1-x}T_xS_2$ as a function of composition x is calculated, which is calculated with respect to pure MoS_2 and TS_2:

$$\Delta H_{\mathrm{m}} = E(\mathrm{Mo}_{1-x}\mathrm{T}_x\mathrm{S}_2)\text{-}(1\text{-}x)E(\mathrm{MoS}_2) - xE(\mathrm{TS}_2) \qquad (4)$$

As shown in Fig. 3(a), although the quasi-binary alloys $Mo_{1-x}W_xS_2$ possess negative mixing enthalpies, the absolute value are very small (maximum 0.005 eV at x=0.5). The reason for the small mixing enthalpies of $Mo_{1-x}W_xS_2$ may come from the similarity of good lattice match between MoS_2 and WS_2. In fact, the random alloying of hetero atoms in mixed $Mo_{1-x}W_xS_2$ throughout the entire chemical compositions ($0<x<1$) have been recently revealed by scanning transmission electron microscope (STEM) images by different authors.[35,36] Our calculations give a clear explanation for the previous experiments on $Mo_{1-x}W_xS_2$ from the theoretical view. The single-layer VS_2 is a special TMD because it is metallic and ferromagnetic, which is very different from MoS_2. The single-layer CrS_2 has good electronic structure similarity with MoS_2 (both are semiconductors), but the lattice mismatch +4%. $Mo_{1-x}V_xS_2$ alloys have the largest mixing enthalpies. The positive mixing enthalpies indicate $Mo_{1-x}V_xS_2$ and $Mo_{1-x}Cr_xS_2$ have a tendency of phase segregation at low temperatures.

The phase stability of $Mo_{1-x}T_xS_2$ alloys is crucial for alloy designing, which can be studied from the mixing free energy. The mixing Helmholtz free energy instead of Gibbs free energy is used to study the phase segregation of the solid solutions. According to regular-solution model, the mixing Helmholtz free energy is described as $\Delta F_m = \Delta H_m - \Delta S_m T$, where ΔH_m, ΔS_m, and T represent the mixing enthalpy, mixing entropy, and thermodynamic temperature, respectively. It should be noted that

temperature-dependent vibration contribution to free energy due to differences in the phonon densities of states, which may affect the relative stability but is not considered here. The mixing enthalpies at various compositions were fitted by a second-order polynomial $\Delta H_m=\Omega x(1-x)$ based on the quasi-chemical model, where Ω is called interaction energy. In order to study the dependence of Ω on x, the values of the mixing enthalpies are fitted by the polynomial $\Delta H_m = B_0+B_1x-B_2x^2$. The results shown that B_0 approaches to zero, and B_1 and B_2 are almost equal. Thus, Ω is considered to be a constant independent on x and equals to B_1 *or* B_2. The mixing entropy is evaluated by $\Delta S_m=-R[x\ln x+(1-x)\ln(1-x)]$. Thus, the mixing Helmholtz free energy can be written as $\Delta F_m=\Omega x(1-x)+RT[x\ln x+(1-x)\ln(1-x)]$. The binodal solubility curve (immiscibility gap) and spinodal decomposition curve for alloys have been investigated by simple formula $\partial F_m/\partial x=0$ *and* $\partial^2 Fm/\partial x^2=0$, which are calculated by $RT[\ln x-\ln(1-x)]+(1-2x)\Omega=0$ and $RT-2x(1-x)\Omega=0$.

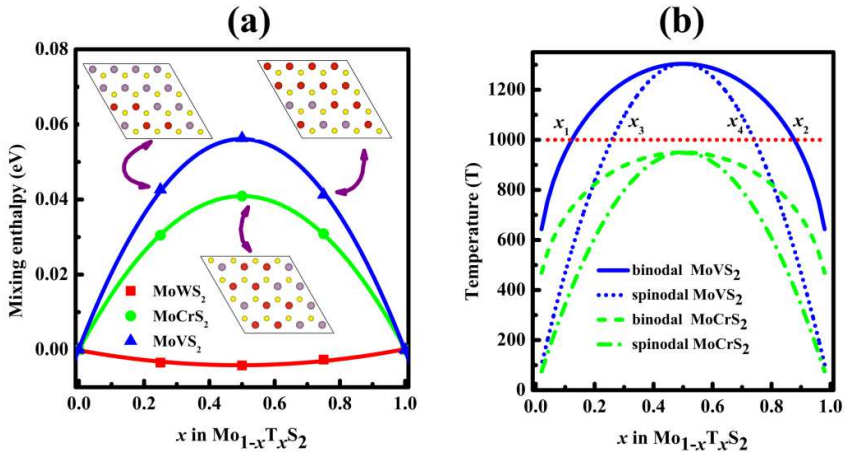

Fig. 3 *(a) The mixing enthalpies and (b) quasi-binary phase diagrams of TMDs alloys (*$Mo_{1-x}W_xS_2$, $Mo_{1-x}Cr_xS_2$, $Mo_{1-x}V_xS_2$*). The corresponding atomic configurations for different compositions are shown in inserts of (a). In (b), the binodal and spindoal curves are shown in blue and green color, respectively.*

The quasi-binary phase diagrams are depicted in Fig. 3 (b). The binodal and spinodal curves meet at x=0.5 at a critical temperature $T_c=\Omega/2R$. At a specific temperature below T_c ($T=T_k<Tc$), homogenous alloys of MoS_2 and TS_2 can still form with low solubility ($0<x<x_1$ *and* $x_2<x<1$). When the composition across the binodal curve ($x_1<x<x_2$), $Mo_{1-x}T_xS_2$ alloys become unstable. They decompose into two phases with the composition of x_1 and x_2. When the temperature is higher than T_c, the large entropy of solid solutions suppresses the positive mixing enthalpy. The immiscibility gap begins to disappear at T_c. The single-layer $Mo_{1-x}T_xS_2$ homogenous alloys become stable in the whole compositions. For $Mo_{1-x}Cr_xS_2$ and $Mo_{1-x}V_xS_2$, T_c is 950 K and 1304 K，respectively. The critical temperature of $Mo_{1-x}V_xS_2$ is higher than that of $Mo_{1-x}Cr_xS_2$，stemming from the more positive mixing enthalpy for the former than the latter.

3.4 Band structures for alloys and heterostructures

Although we predict that the most stable configuration is either alloys or heterostructures, it should be noted that the final configuration will greatly be affected by the synthesis technique, such as the quenching speed. MoS_2-WS_2 heterostructures should occur as metastable phases due to high diffusion energy barrier to overcome in non-defective lattice at room temperature. From this view, both TMDs alloys and heterostructures should be fabricated in practice. The two different kinds of TMDs composites are expected to affect the electronic structure of TMDs. In the following, the electronic structures of both $Mo_{1-x}T_xS_2$ alloys and MoS_2-TS_2 heterostructures (T=W, Cr, and V) are investigated.

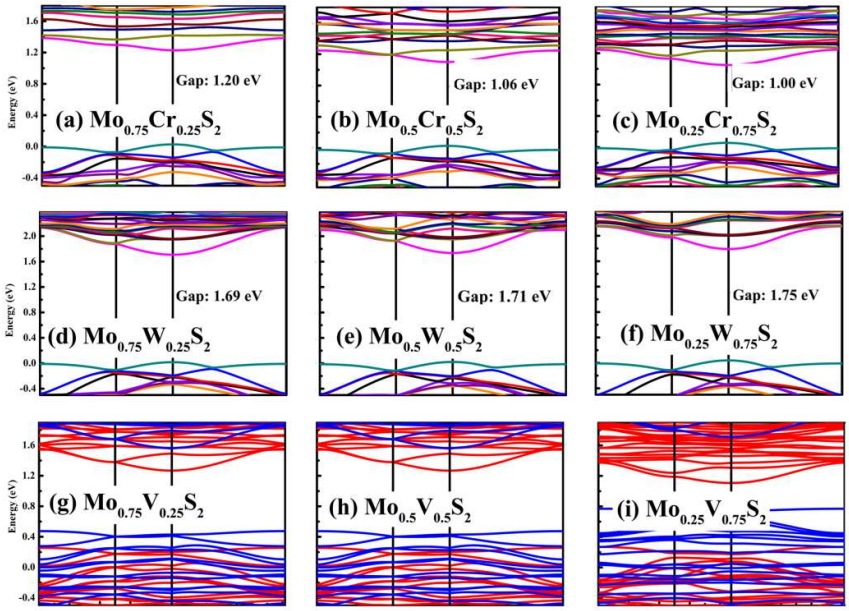

Fig. 4 *Band structures for alloyed TMDs at the different compositions: (a)-(c)* $Mo_{1-x}W_xS_2$, (d)-(f) $Mo_{1-x}Cr_xS_2$, and (g)-(i) $Mo_{1-x}V_xS_2$. *In (a)-(f), different band dispersions for* $Mo_{1-x}Cr_xS_2$ *and* $Mo_{1-x}Cr_xS_2$ *are depicted as various colors, for* $Mo_{1-x}V_xS_2$, *(g)-(i), the red and blue color are used to distinguish spin-up and spin-down states, respectively.*

The electronic structures of $Mo_{1-x}T_xS_2$ alloys (T=W, Cr, and V) are shown in Fig. 4. The band gaps of MoS_2 could be tuned by alloying foreigner metal atoms. The $Mo_{1-x}Cr_xS_2$ and $Mo_{1-x}W_xS_2$ solutions remain direct-band-gap semiconducting as the constituents of MoS_2, CrS_2, and WS_2. The $Mo_{1-x}V_xS_2$ alloys are metallic due to the energy bands crossing the Fermi surface. In addition, $Mo_{1-x}V_xS_2$ alloys are ferromagnetic shown by spin-splitting in Fig. 4((g)-(i)) with magnetic moment concentrating on V atoms. In order to check the ground state of V-containing systems, more calculations are made on $Mo_{0.75}V_{0.25}S_2$. The results show that the ferromagnetic state is energetically favorable by 25 meV than the nonmagnetic one. Further calculations are made by flipping the spin direction of V atoms. In the $Mo_{0.75}V_{0.25}S_2$,

it contains 4 V atoms in the supercell, and there are 4 possible cases by flipping the spin direction of one V atoms, and 6 possible cases by flipping the spin direction of two V atoms. The energies of two cases with the spin direction of two V atoms slipped have equal energies, 35 meV higher than the ferromagnetic state. The other cases have identical energies with the ferromagnetic state with all spins in the same direction. $Mo_{0.75}V_{0.25}S_2$ has been carefully demonstrated to be ferromagnetic.

The single-layer MoS_2 can retain semiconducting or change to be metallic by alloyed with different chosen TMDS. The band gap of MoS_2 can either be reduced or be enhanced via alloyed with other TMDs possessing smaller or larger bang gap than MoS_2. The band gaps are continuously associated with the constitute composition x in $Mo_{1-x}T_xS_2$ alloys. The single-layer MoS_2 can have so many distinct electronic structures, band-gap-varying semiconducting and metallic, which depends on the alloyed TMDs type and chemical composition. Further, as mentioned above, the pure DFT may have problem in the calculating the band gap, especially for the Cr and V systems. In order to check the reliability of such calculations, the typical alloys, $Mo_{0.75}V_{0.25}S_2$ and $Mo_{0.75}Cr_{0.25}S_2$, are further calculated with DFT+U method. During our calculations on both $Mo_{0.75}V_{0.25}S_2$ and $Mo_{0.75}Cr_{0.25}S_2$, U and J (U= 5.95 eV and J = 0.95 eV) for V and Cr were taken from the reference 51. As shown in Fig. S3, the $Mo_{0.75}V_{0.25}S_2$ is ferromagnetic and metallic, and $Mo_{0.75}Cr_{0.25}S_2$ is still semiconducting and nonmagnetic, as predicted by PBE. It should be noted that the bandgap of $Mo_{0.75}Cr_{0.25}S_2$ may be affected by the larger U or hybrid functional, such as PBE0.

The armchair and zigzag heterostructures are originally chosen with equal number of atoms in the unit cell but consequently have different widths of the strips. The widths of armchair and zigzag MoS_2-WS_2 are 12.7 Å and 22 Å, respectively. We refer these two heterostructure as AHS MoS_2-WS_2 and ZHS MoS_2-WS_2, respectively. The electronic structures of MoS_2-TS_2 heterostructures are also shown in Fig. 5. The MoS_2-WS_2 and MoS_2-CrS_2 heterostructures are semiconducting whereas MoS_2-VS_2 ones are metallic. All alloys and heterostructures keep semiconducting as single-layer MoS_2 but become metallic when V atoms are introduced. In order to know the width effect, another armchair MoS_2-WS_2 heterostructure with the strip of 22 Å (same to that of zigzag one) is further calculated. In the following we refer this strip as AHS-1 MoS_2-WS_2. The results (see Fig. S2) show that both the zigzag and armchair heterostructures give nearly the same band gap, which suggests that width of the strip greatly affects the band structure.

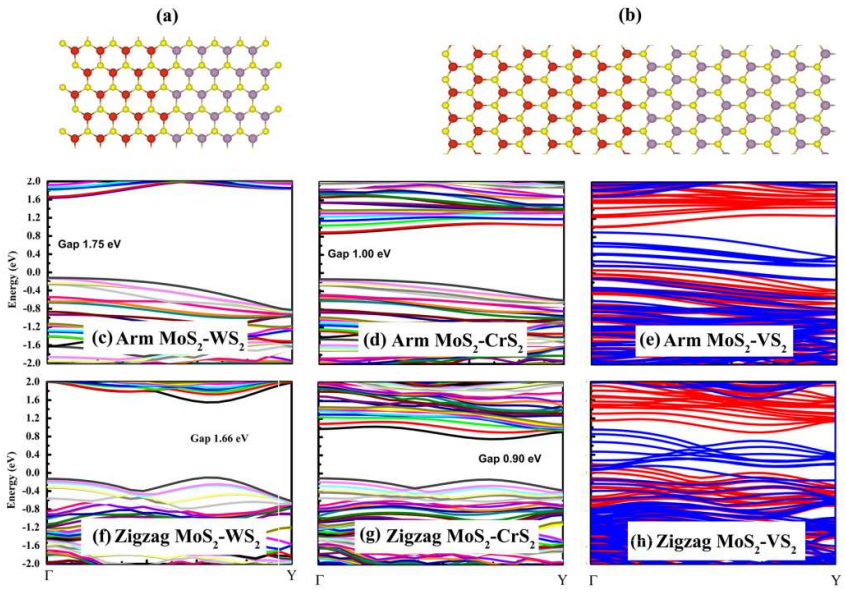

Fig. 5 *The atomic structures of heterostructures for the different types: (a) armchair and (b) zigzag; Band structures of the heterostructrues are shown for both armchair and zigzag types in (c)-(h): (c) and (f) MoS_2-WS_2, (d) and (g) MoS_2-CrS_2, and (e) and (h) MoS_2-VS_2. The upper panels are armchair and low panels are zigzag one. The widths of the strips are* 12.7 Å for armchair and 22 Å for zigzag MoS_2-WS_2.

3.5 Photocatalytic ability

The above discussions have demonstrated that the single layer of TMDs for both alloys and heterostructures except MoS_2-VS_2 exhibits the characteristic of direct-band-gap compared with pure TS_2. Such results clearly suggest greatly enhanced optical absorption of both single-layer TMDs alloys and heterostructures because no phonons are required for this optical transition process. The gaps of different kinds of TMDs have a decent band gap range, from 0.89 to1.87 eV, which allow absorption of a significant percentage of the visible light. Thus such two-dimensional materials have great potential implications in high-effective solar energy conversion, such as solar energy cells and photocatalytic water splitting.

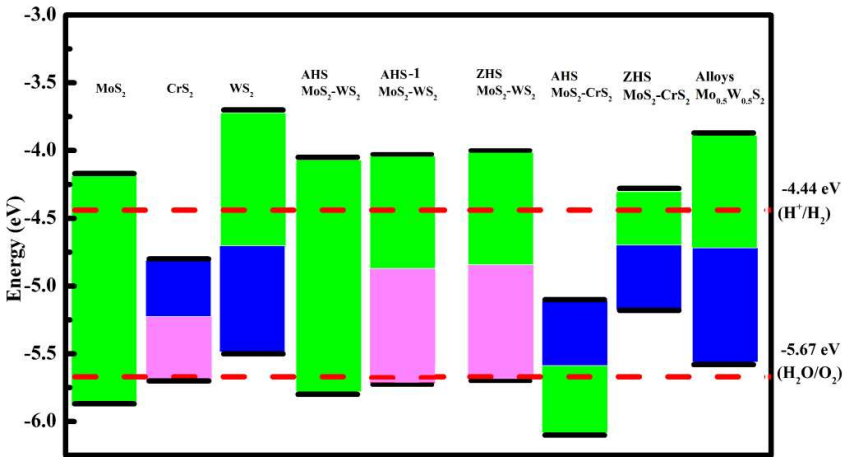

Fig. 6 *Band alignments of VBM and CBM for the pure MoS_2, CrS_2, WS_2, $Mo_{0.5}W_{0.5}S_2$ alloy and heterostructures(AHS MoS_2-WS_2, ZHS MoS_2-WS_2, AHS MoS_2-CrS_2, AHS-1 MoS_2-WS_2, and ZHS MoS_2-CrS_2). Here AHS and ZHS represent armchair and zigzag typed heterostructures, respectively. AHS MoS_2-WS_2 is calculated with the width of 12.7 Å strip, and AHS-1 MoS_2-WS_2 is calculated with 22 Å strip. The two horizontal red lines indicate the water reduction (H^+/H_2) and oxidation (H_2O/O_2) potentials, respectively. The different colors depict diverse photo activity on the two reactions of water split (down) and H_2 production (upper). Green, pink and blue indicate materials have good, bad and incapable photocatalytic activity of the reactions, respectively.*

As a decent photocatalytic material for water splitting, it not only requires a suitable band gap, but also an appropriate band gap position. A good photocatalytic material for water-splitting requires valence band maximum (VBM) energy lower than the oxidation potential (-5.67) of H_2O/O_2, and conduction band minimum (CBM) energy higher than the reduction potential (-4.44 eV) of H^+/H_2. Fig. 6 shows the CBM and VBM energy levels with respect to vacuum energy level for pure TMDs, heterostructures, and alloys. Neither WS_2 nor CrS_2 is a good photocatalytic material due to the unsuitable band alignments. MoS_2 is a good candidate for both the oxidation and reduction reactions due to the reasonable band edge requirement, as found in the previous calculations[53]. It should be noted that both alloys and heterostructures can not only change the band gap but also shifts band edge position of TMDs. Among all the heterostructures and alloys, only MoS_2-WS_2 heterostructures exhibit reasonable band edge position for water splitting.

The contributions of band edge charges of both armchair and zigzag MoS_2-WS_2 and MoS_2-CrS_2 heterostructures are further explored. The density distributions of CBM and VBM for heterostructures are shown in Fig. 7**.** In the case of MoS_2-WS_2 heterostructures, the VBM and CBM charges are completely separated: VBM is localized on WS_2 side and CBM concentrates on MoS_2 side for both armchair and zigzag ones (Fig. 7(a) and (b)). The VBM and CBM charges of armchair MoS_2-CrS_2 heterostructures concentrate on CrS_2 side (Fig. 7(c)). The result demonstrates that the photo-generated electron and hole are spontaneously separated for MoS_2-WS_2

heterostructures, which can suppress charge recombination and dramatically enhance the photocatalytic efficiency.

It should be noted that width of the strip greatly affects the position of band edge position. The AHS MoS_2-WS_2 (the strip width of 13 Å) shows a suitable band position for both reduction and oxidation, while AHS-1 MoS_2-WS_2 (the strip width of 22 Å) does not have a suitable band position. Recently Conesa provided a good principle for analyzing the band alignment in heterostructures.[54]. Rather than using that method, in this paper we clarify the positions of the VBM and CBM from the projected densities of states (PDOS) for metal atoms in AHS as depicted in Fig. S4. In pure MoS_2 and WS_2, VBM mainly comes from d_{xy} and $d_{x^2-y^2}$ orbits for both pure TMDs, but CBM from d_{z^2} orbital (Fig. S3(a) and (b)). In armchair heterostructure, the energy of d_{z^2} orbital fairy below the Fermi energy of both of Mo and W atoms become higher than d_{xy} and $d_{x^2-y^2}$ orbits (Fig. S3(c) and (d)). As shown in Fig. S3(e), the VBM and CBM are contributed by the d_{z^2} orbital of W and Mo atoms, respectively. Such result clearly reveals the origin of the extraordinary electronic properties of electron-hole separation.

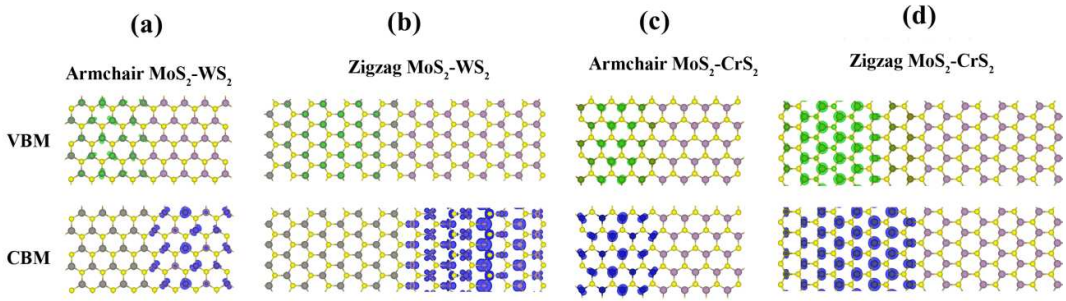

Fig. *7 Charge densities of VBM (green) and CBM (blue) with an isosurface value of 0.008 e/Å^3 for TMDs heterostructures: (a) armchar MoS_2-WS_2, (b) zigzag MoS_2-WS_2, (c) armchair MoS_2-CrS_2, and (d) zigzag MoS_2-CrS_2. The upper panels are charge densities of VBM, and low panels are the charge density of CBM. The purple, gray, dark green and yellow colors represent the Mo, W, Cr and S atoms, respectively.*

Although pure photocatalysts have been tremendously studied, they often suffer many shortcomings, such as the high recombination rate of photo-generated electronics-hole pairs, which causes the low efficiency limiting the practical application of the photocatalytic materials, such as g-C_3N_4 and TiO_2.[55,56] Consequently avoiding electronics-hole pair recombination is critical for photocatalytic activity. Forming heterostructures with different semiconductors is a feasible route to inhibit the recombination of electron–hole pairs arising from the

charge separation. The calculations suggest fabricating heterostructures in experiments could induce to electron–hole separations. In particular, the MoS_2-WS_2 heterostructures are the best photocatalysts among the entire composites for H_2 production.

4. Conclusions

The atomic structures and electronics properties of mixed alloys or heterostructures of TMDs with single-layer MoS_2 are carefully examined using DFT calculations. The formation energies change monotonously with the number of neighboring homo-atom bonds. The three alloy systems, $Mo_{1-x}W_xS_2$ or $Mo_{1-x}Cr_xS_2$ and $Mo_{1-x}V_xS_2$, exhibit distinct atom arrangements preference of hetero (Mo-W) atoms in the first alloys and homo (Mo-Mo, Cr-Cr, and V-V) atoms in the latter two alloys. The calculated quasi-binary phase diagrams further display high phase stability for $Mo_{1-x}W_xS_2$ but severe phase segregation for MoS_2-CrS_2 and MoS_2-VS_2. Further electronic structure studies reveal that band structure of MoS_2 can be effectively tuned by either alloying or heterostructure, and the corresponding band gaps are around 0.89~1.87 eV. More interestingly, heterostructures not only can modulate the band gap, but also adjust band edge position to meet the requirement of photocatalystic water-splitting and electron-hole separation, which strongly enhance the photocatalytic activity. The MoS_2-WS_2 heterostructure not only has the reasonable band gap and band edge position for hydrogen generation, but the unique electronic structure of spontaneous electron-hole separation.

Acknowledgments

This work was supported by the National Natural Science Foundation of China (No. 51222212 and 11204262), the CAEP foundation (Grant No. 2012B0302052), the MOST of China (973 Project, Grant NO. 2011CB922200). The computations supports from Informalization Construction Project of Chinese Academy of Sciences during the 11th Five-Year Plan Period (No.INFO-115-B01) are also highly acknowledged.

References

1 K. S. Novoselov; A. K. Geim; S. V. Morozov; D. Jiang; Y. Zhang; S. V. Dubonos; I. V. Grigorieva; A. A. Firsov *Science* 2004, **306**, 666.
2 W.-J. Yin; Y.-E. Xie; L.-M. Liu; R.-Z. Wang; X.-L. Wei; L. Lau; J.-X. Zhong; Y.-P. Chen *J. Mater. Chem. A* 2013, **1**, 5341.
3 X. G. Luo; L.-M. Liu; Z. P. Hu; W.-H. Wang; W.-X. Song; F. F. Li; S.-J. Zhao; H. Liu; H.-T. Wang; Y. J. Tian *J. Phys. Chem. Lett.* 2012, **3**, 3373.
4 Y. C. Wang; M. S. Miao; J. Lv; L. Zhu; K. T. Yin; H. Y. Liu; Y. M. Ma *J. Chem. Phys.* 2012, **137**, 224108.
5 J. F. Gao; J. J. Zhao; F. Ding *J. Am. Chem. Soc.* 2012, **134**, 6204.
6 T. Cheiwchanchamnangij; W. R. L. Lambrecht *Phys. Rev. B* 2012, **85**, 205302.
7 A. Kuc; N. Zibouche; T. Heine *Phys. Rev. B* 2011, **83**, 245213.
8 K. F. Mak; C. Lee; J. Hone; J. Shan; T. F. Heinz *Phys. Rev. Lett.* 2010, **105**, 136805.

9 A. Splendiani; L. Sun; Y. Zhang; T. Li; J. Kim; C.-Y. Chim; G. Galli; F. Wang *Nano Lett.* 2010, **10**, 1271.
10 G. Eda; H. Yamaguchi; D. Voiry; T. Fujita; M. Chen; M. Chhowalla *Nano Lett.* 2011, **11**, 5111.
11 H. Zhang; X.-B. Li; L.-M. Liu *J. Appl. Phys.* 2013, **114**, 093710.
12 M. Chhowalla; H. S. Shin; G. Eda; L.-J. Li; K. P. Loh; H. Zhang *Nature Chem.* 2013, **5**, 263.
13 H. Zhang; L.-M. Liu; W.-M. Lau *J. Mater. Chem. A* 2013, **1**, 10821.
14 H. R. Gutiérrez; N. Perea-López; A. L. Elías; A. Berkdemir; B. Wang; R. Lv; F. López-Urías; V. H. Crespi; H. Terrones; M. Terrones *Nano Lett.* 2012, **13**, 3447.
15 H. I. Karunadasa; E. Montalvo; Y. Sun; M. Majda; J. R. Long; C. J. Chang *Science* 2012, **335**, 698.
16 H. Hwang; H. Kim; J. Cho *Nano Lett.* 2011, **11**, 4826.
17 B. Radisavljevic; A. Radenovic; J. Brivio; V. Giacometti; A. Kis *Nat Nano* 2011, **6**, 147.
18 S. S. Chou; M. De; J. Kim; S. Byun; C. Dykstra; J. Yu; J. Huang; V. P. Dravid *J. Am. Chem. Soc.* 2013, **135**, 4584.
19 H. Shi; H. Pan; Y.-W. Zhang; B. I. Yakobson *Phys. Rev. B* 2013, **87**, 155304.
20 Y. Y. Hui; X. Liu; W. Jie; N. Y. Chan; J. Hao; Y.-T. Hsu; L.-J. Li; W. Guo; S. P. Lau *ACS Nano* 2013, **7**, 7126.
21 H. Conley; B. Wang; J. Ziegler; R. F. Haglund; S. T. Pantelides; K. I. Bolotin *Nano Lett.* 2013, **13**, 3626.
22 K. Dolui; C. D. Pemmaraju; S. Sanvito *ACS Nano* 2012, **6**, 4823.
23 Y. F. Li; D. H. Wu; Z. Zhou; C. R. Cabrera; Z. F. Chen *J. Phys. Chem. Lett.* 2012, **3**, 2221.
24 Y. F. Li; Z. Zhou; S. B. Zhang; Z. F. Chen *J. Am. Chem. Soc.* 2008, **130**, 16739.
25 L. Z. Kou; C. Tang; Y. Zhang; T. Heine; C. F. Chen; T. Frauenheim *J. Phys. Chem. Lett.* 2012, 2934.
26 W. Zhou; X. Zou; S. Najmaei; Z. Liu; Y. Shi; J. Kong; J. Lou; P. M. Ajayan; B. I. Yakobson; J.-C. Idrobo *Nano Lett.* 2013, **13**, 2615.
27 A. N. Enyashin; M. Bar-Sadan; L. Houben; G. Seifert *J. Phys. Chem. C* 2013, **117**, 10842.
28 H.-P. Komsa; J. Kotakoski; S. Kurasch; O. Lehtinen; U. Kaiser; A. V. Krasheninnikov *Phys. Rev. Lett.* 2012, **109**, 035503.
29 X. Zou; Y. Liu; B. I. Yakobson *Nano Lett.* 2012, **13**, 253.
30 S. Najmaei; Z. Liu; W. Zhou; X. Zou; G. Shi; S. Lei; B. I. Yakobson; J.-C. Idrobo; P. M. Ajayan; J. Lou *Nature Mater.* 2013, **12**, 754.
31 S. Bertolazzi; D. Krasnozhon; A. Kis *ACS Nano* 2013, **7**, 3246.
32 Y. Li; H. Wang; L. Xie; Y. Liang; G. Hong; H. Dai *J. Am. Chem. Soc.* 2011, **133**, 7296.
33 Q. Xiang; J. Yu; M. Jaroniec *J. Am. Chem. Soc.* 2012, **134**, 6575.
34 X. Zong; H. J. Yan; G. P. Wu; G. J. Ma; F. Y. Wen; L. Wang; C. Li *J. Am. Chem. Soc.* 2008, **130**, 7176.
35 D. O. Dumcenco; H. Kobayashi; Z. Liu; Y.-S. Huang; K. Suenaga *Nature Commun.*

2013, **4**, 1351.
36 Y. F. Chen; J. Y. Xi; D. O. Dumcenco; Z. Liu; K. Suenaga; D. Wang; Z. G. Shuai; Y.-S. Huang; L. M. Xie *ACS Nano* 2013, **7**, 4610.
37 H.-P. Komsa; A. V. Krasheninnikov *J. Phys. Chem. Lett.* 2012, **3**, 3652.
38 K. Kośmider; J. Fernández-Rossier *Phys. Rev. B* 2013, **87**, 075451.
39 J. Kang; S. Tongay; J. Zhou; J. Li; J. Wu *Appl. Phys. Lett.* 2013, **102**, 012111.
40 H. Terrones; F. López-Urías; M. Terrones *Sci. Rep.* 2013, **3**, 1549.
41 Y. Gao; Y. Zhang; P. Chen; Y. Li; M. Liu; T. Gao; D. Ma; Y. Chen; Z. Cheng; X. Qiu; W. Duan; Z. Liu *Nano Lett.* 2013, **13**, 3439.
42 L. Ci; L. Song; C. Jin; D. Jariwala; D. Wu; Y. Li; A. Srivastava; Z. F. Wang; K. Storr; L. Balicas; F. Liu; P. M. Ajayan *Nat Mater* 2010, **9**, 430.
43 K. Yuge *Phys. Rev. B* 2009, **79**, 144109.
44 G. Kresse; J. Furthmüller *Phys. Rev. B* 1996, **54**, 11169.
45 G. Kresse; J. Furthmüller *Comp. Mater. Sci.* 1996, **6**, 15.
46 G. Kresse; D. Joubert *Phys. Rev. B* 1999, **59**, 1758.
47 J. P. Perdew; K. Burke; M. Ernzerhof *Phys. Rev. Lett.* 1996, **77**, 3865.
48 H. J. Monkhorst; J. D. Pack *Phys. Rev. B* 1976, **13**, 5188.
49 A. Zunger; S. H. Wei; L. G. Ferreira; J. E. Bernard *Phys. Rev. Lett.* 1990, **65**, 353.
50 Y. D. Ma; Y. Dai; M. Guo; C. W. Niu; Y. T. Zhu; B. B. Huang *ACS Nano* 2012, **6**, 1695.
51 M. Ramzan; R. Ahuja *Appl. Phys. Lett.* 2011, **99**, 221904.
52 A. Ramasubramaniam *Phys. Rev. B* 2012, **86**, 115409.
53 H. L. Zhuang; R. G. Hennig *Chem. Mater.* 2013, **25**, 3232.
54 J. C. Conesa *J. Phys. Chem. C* 2012, **116**, 18884.
55 Y. Zhang; T. Mori; J. Ye; M. Antonietti *J. Am. Chem. Soc.* 2010, **132**, 6294.
56 Y.-F. Li; Z.-P. Liu *J. Am. Chem. Soc.* 2011, **133**, 15743.

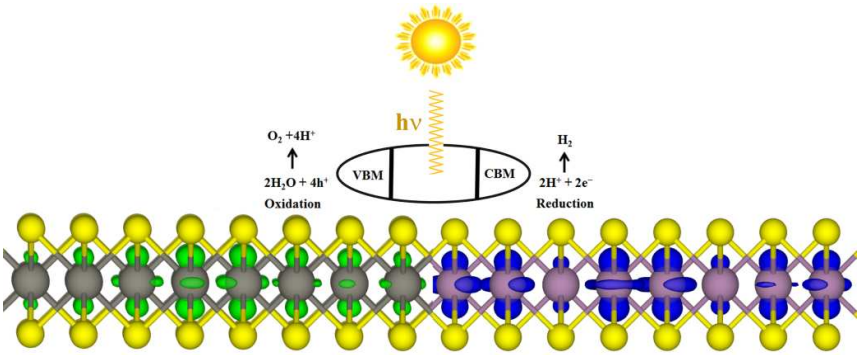

Graphic Abstract *Charge density of VBM (green) and CBM (blue) for armchair MoS_2-WS_2 heterostructures, indicating the spontaneously separation of photo-generated electronics and holes, which could strongly enhance the photocatalytic activity due to suppressing the electronic-hole recombination.*